Inhomogeneous shear flows in soft jammed materials with tunable attractive forces

Pinaki Chaudhuri,[1] Ludovic Berthier,[2] and Lydéric Bocquet[1]
[1]*Laboratoire PMCN, Université Claude Bernard Lyon 1, Villeurbanne, France*
[2]*Laboratoire Charles Coulomb, UMR 5221, CNRS and Université Montpellier 2, Montpellier, France*
(Received 25 November 2011; published 21 February 2012)

We perform molecular dynamics simulations to characterize the occurrence of inhomogeneous shear flows in soft jammed materials. We use rough walls to impose a simple shear flow and study the athermal motion of jammed assemblies of soft particles in two spatial dimensions, both for purely repulsive interactions and in the presence of an additional short-range attraction of varying strength. In steady state, pronounced flow inhomogeneities emerge for all systems when the shear rate becomes small. Deviations from linear flow are stronger in magnitude and become very long lived when the strength of the attraction increases, but differ from permanent shear bands. Flow inhomogeneities occur in a stress window bounded by the dynamic and static yield stress values. Attractive forces enhance the flow heterogeneities because they accelerate stress relaxation, thus effectively moving the system closer to the yield stress regime where inhomogeneities are most pronounced. The present scenario for understanding the effect of particle adhesion on shear localization, which is based on detailed molecular dynamics simulations with realistic particle interactions, differs qualitatively from previous qualitative explanations and *ad hoc* theoretical modeling.

DOI: 10.1103/PhysRevE.85.021503 PACS number(s): 83.10.Rs, 83.50.−v, 62.20.−x, 83.60.La

I. INTRODUCTION

Soft jammed materials, such as dense emulsions, foams, and pastes, are ubiquitous in nature and have a wide range of industrial applications [1,2]. Normally, these materials only flow when an externally applied stress exceeds a critical value, the "yield stress," while they behave as a soft solid otherwise. Thus the flow properties of these systems are intrinsically nonlinear and exhibit complex features that challenge both experimentalists and theoreticians [3]. To understand the rheology of these complex fluids, we want to know the mechanical response of the system to an externally applied force. However, this becomes a highly nontrivial task when the response is not spatially homogeneous, or when it occurs over a broad range of time scales. These two challenging factors routinely characterize the rheology of soft jammed materials, emphasizing the need for spatially and temporally resolved studies of the flow properties in dense particulate systems under shear [4]. Clearly, molecular dynamics simulations are well suited to pursue this task, because they naturally combine particle resolution with the possibility to simulate large systems with controlled interactions over relatively long times.

In typical experimental conditions, a broad variety of complex fluids display spatially inhomogeneous flows, usually described as "shear bands," even though this single name in fact hides a diversity of distinct phenomena [4,5]. In this paper, we are specifically interested in the flow behavior of dense assemblies of large spherical particles that form athermal disordered solids, and we primarily think of foams, emulsions, and dense colloidal suspensions as relevant experimental realizations of our numerical model [4]. While early experiments commonly reported the existence of inhomogeneous shear-banded flows in foams and dense emulsions, more recent work [6–8] has established that, when properly prepared and studied over sufficiently long times, shear bands in dense systems of soft repulsive particles do not appear as a permanent phenomenon, although flow inhomogeneities may appear to be extremely long lived in some cases [7]. Recently, however, it was reported in several instances that the addition of a small amount of attractive forces between particles triggers the appearance of shear bands [8–11]. A common interpretation is that shear bands in this case result from thixotropic behavior competing with the imposed flow [12]. While natural for low-density colloidal gels which have a complex structure [13,14], this explanation appears less convincing for jammed systems, which present instead a fairly homogeneous structure.

Shear-banding phenomena have been observed also in numerical simulations of amorphous solids under flow [15,16]. It was initially reported for a sheared Lennard-Jones mixture [17], where it was argued that the coexistence of flowing and static phases results from the existence of distinct bounds for static and dynamic yield stresses leading to a multivalued flow curve [18]. Subsequently, in studies of model metallic glasses [19], shear banding was observed using a variety of boundary conditions, quench rates, or systems sizes, which motivated theoretical extensions of the shear-transformation zone model [20] to account for shear bands [21]. However, in experiments performed on actual metallic glasses, these flow inhomogeneities evolve rapidly with the applied deformation and the system develops fractures before a steady state can be reached. In a parallel effort, studies of athermal quasistatic shear flow of amorphous solids have revealed the existence of system-spanning avalanches generated by correlated activation of plastic events [22,23]. These observations seem to be in tune with the generic scenario that dynamical heterogeneities are a characteristic feature of amorphous materials [16]. Although it is tempting to speculate that dynamic heterogeneities, avalanches, and shear bands are various facets of the same underlying physics, more precise links between these phenomena are missing [15].

At the theoretical level, many early models developed to account for the rheology of soft amorphous materials were mean field in nature, and spatial fluctuations were usually discarded [24–26]. More recently, several coarse-grained models have emerged that attempt to capture the idea, revealed by

 ©2012 American Physical Society

the above-mentioned numerical studies, that plastic events are localized but may trigger additional plastic events elsewhere in the system, thus cascading into sustained flow [27–31]. While such modeling directly yields spatially inhomogeneous dynamics, the appearance of permanent shear bands does not necessarily follow. Numerical simulations of these models indeed do not produce genuine shear bands [27,28], which seems to suggest that shear bands might only occur under quite specific conditions. Several recent studies of simple models suggest that some form of long-lived shear-banding phenomena may occur after shear startup [21,32,33]. These approaches also build on the possibility to observe distinct static and dynamic yield stress values, the former being enhanced by prolonged aging in thermal glasses.

Several mechanisms have been put forward to account for permanent flow inhomogeneities, which typically revolve around the idea that the stress-strain rate flow curve, $\sigma = \sigma(\dot{\gamma})$, is multivalued. We already mentioned the possibility, first discussed in Refs. [17,18], that the flow curve at finite shear rates is monotonic [for instance, of the Herschel-Bulkley type with a finite dynamic yield stress, $\sigma_d = \lim_{\dot{\gamma}\to 0}\sigma(\dot{\gamma})$], but that there exists a static branch at $\dot{\gamma} = 0$ extending up to a static yield stress value σ_s larger than the dynamic one, $\sigma_s > \sigma_d$. This opens a finite range of stress where the shear rate can take two values. Genuine nonmonotonic flow curves have recently been obtained in various models by including the generic idea that yielding dynamics should be self-consistently connected to the evolution of the local structure. This was done, for instance, using self-consistent dynamics of the effective temperature [34] in the soft glassy rheology model [24,35], or by incorporating thixotropic effects using an additional time scale for structural "restructuration" in schematic [36] or coarse-grained models [29,37,38], in which case nonmonotonic flow curves arise when structural recovery is slower than the characteristic relaxation time of the system. This hypothesis was, however, not justified by microscopic arguments or detailed measurements. Alternatively, it has been proposed that shear banding could also occur due to a shear-concentration coupling [39], with the possibility that at small enough shear rates, variations in local concentrations would result in the large fluctuations in flow rates. Clearly, more numerical and experimental studies are now necessary in order to test and discriminate these different physical ideas.

In this paper, we report two-dimensional simulational studies of the athermal flow of highly jammed systems, consisting of particles having either purely repulsive interactions (as in foams [6] and simple emulsions [8,9]), or having both repulsive and short-range attractions (as in adhesive emulsions [8–11]). Motivated by the phenomonological finding that attractive forces might be responsible for the appearance of permanent shear bands, we specifically check whether changing interactions results in different shear localization properties during steady-state flow, and use our spatially and temporally resolved simulations to seek a physical interpretation of our findings. We find that strong flow inhomogeneities are present in all systems, except that the lifetime and degree of fluctuations are indeed much higher with increased attractions, but we do not observe simple, permanent shear bands even in our most adhesive systems. We find instead that attractive forces, by accelerating stress relaxation, effectively shift the system closer toward the yield stress regime where flow inhomogeneities can become so pronounced that the system is not able to sustain a linear flow profile. Such a theoretical scenario was not anticipated in any of the above-mentioned work.

The paper is organized as follows. In Sec. II we describe our model and numerical methods. We then present our measurements and results in Sec. III, and we discuss our results in Sec. IV. We conclude the paper in Sec. V.

II. MODELS AND NUMERICAL METHODS

A. Repulsive interactions

The model system that we study is a collection of polydisperse soft particles, introduced as a model for foams [40,41], and which has now been extensively studied to understand the physics of jammed soft materials [1] both in athermal conditions [42,43] and at finite temperatures [44]. In the repulsive case, two particles, having diameters d_i and d_j, interact via a harmonic potential:

$$V(r_{ij}) = \begin{cases} \epsilon\left(1 - \frac{r_{ij}}{d_{ij}}\right)^2, & r_{ij} < d_{ij}, \\ 0, & r_{ij} > d_{ij}, \end{cases} \tag{1}$$

where $d_{ij} = (d_i + d_j)/2$. We choose a 50:50 binary mixture for the polydispersity with a mean diameter of $\langle d\rangle = 1.0$ and a size ratio of 1.4 to avoid crystallization.

B. Attractive interactions

We introduce adhesive interactions between the particles in a manner similar to models of cohesive granular media [45]. Specifically, we introduce two parameters, ℓ_1 and $\ell_2 > \ell_1$, through which we can control the range and depth of the attractive forces between the particles. We choose the following form for the interparticle interactions:

$$V(r_{ij}) = \begin{cases} \epsilon\left[\left(1 - \frac{r_{ij}}{d_{ij}}\right)^2 - \ell_1\ell_2\right], & \frac{r_{ij}}{d_{ij}} < 1 + \ell_1, \\ \frac{-\epsilon\ell_1}{\ell_2 - \ell_1}\left[1 + \ell_2 - \frac{r_{ij}}{d_{ij}}\right]^2, & 1 + \ell_1 < \frac{r_{ij}}{d_{ij}} < 1 + \ell_2, \\ 0, & \frac{r_{ij}}{d_{ij}} > 1 + \ell_2. \end{cases} \tag{2}$$

This simple form is chosen because it yields an interaction force which is piecewise linear; see Fig. 1.

In our simulations, we use ℓ_2 to fix the range of the interparticle force: $\ell_2 = 0.2$, and change the depth and range of the attractive part by varying ℓ_1. The shape of the interactions, with the inclusion of the attractive part, is illustrated in Fig. 1. By varying the position at distance $(1 + \ell_1)d_{ij}$ of the minimum in the interparticle force, the amplitude of the attractive force is varied, which we quantified by introducing the parameter $u = -2\epsilon\ell_1/d_{ij}$, which sets an energy scale for the attraction strength. We have studied different values of the particle adhesion, $u = 0$, 0.05, 0.10, and 0.15, as shown in Fig. 1. We do not explore larger adhesion strength to avoid the occurrence of any shear-induced phase separation.

C. Simulation methods

We study the shear flow of a two-dimensional system of soft particles. We use very large dimensions for the simulation box, $L_x = 84.46\langle d\rangle$ and $L_y = 99.39\langle d\rangle$, which contains

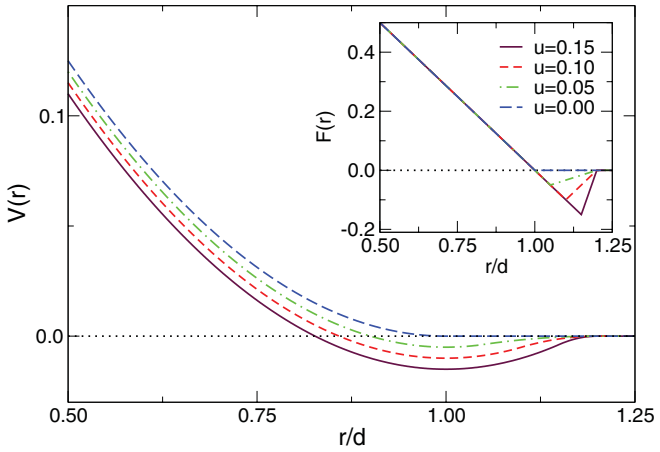

FIG. 1. (Color online) Interparticle potential $V(r)$, Eqs. (1) and (2), for $\epsilon = 1/2$, and tunable strength of attractive forces from $u = 0$ (purely repulsive case) to $u = 0.15$. The range of the attractive forces is constant, $r/d = 1.2$, but the strength increases with u. Inset: The corresponding forces (shown with the same colors) with the labeling for $u = -\ell_1/d$ quantifying the strength of the attractive part.

$N = 10\,404$ particles. By "very large," we mean that the size of the gap is much larger than the smaller gaps studied, for instance, in microfluidic devices [39,46]. Shear is imposed via rough walls constructed as follows. A layer of particles having thickness $2\langle d\rangle$ is frozen both at the top and bottom of the simulation box in the y direction, from an unsheared configuration (i.e., taken in an energy minimum). These rough walls have thus a microstructure which is close to the sheared system, and the same two walls are used throughout this work. In the simulations with attractive forces, we use the same structure for the walls, but implement the same attractive forces for the wall-fluid interactions.

To impose a constant shear rate $\dot\gamma$, we pull the top wall at a velocity fixed by $v_{\rm wall} = \dot\gamma(L_y - 4\langle d\rangle)$, with the bottom wall being kept fixed. We also carry out some shear simulations with an imposed constant stress σ. This is done by pulling the top wall by a tangential force $F = \sigma L_x$ [47,48], with the bottom wall again remaining fixed.

The motion of the particles in the bulk are governed by the conservative forces described above, while athermal behavior is ensured using viscous dissipative forces. During the flow, when two particles overlap, they experience a dissipative force which depends on their relative velocity: $-b[(\vec v_i - \vec v_j)\cdot\hat r_{ij}]\hat r_{ij}$, where $b = 2$ is the damping coefficient, and $\hat r_{ij}$ is the unit vector between particles i and j. The range of the "overlap" used for dissipation is d_{ij} for pairs of purely repulsive particles, and corresponds to $(1 + \ell_2)d_{ij}$ when attractive forces are included.

We work at a constant volume fraction of $\phi = N\pi\langle d^2\rangle/(4V) = 1.0$, which is much beyond the jamming point $\phi_J \sim 0.85$. This implies that the structure is fairly homogeneous and resembles the one of dense amorphous solids. Thus our modeling approach bears no similarities with colloidal gels, which are found to also exhibit shear bands in experimental work [13,14].

The units for energy, length, and time are 2ϵ, $\langle d\rangle$, and $\langle d\rangle/\sqrt{2\epsilon/m}$, respectively, where m is the mass of the particles. The trajectories of the particles are evolved by numerically integrating the corresponding Newton's equations of motion, using a velocity-Verlet scheme [49]. Throughout this work we seek to study velocity profiles of various systems in steady state. Thus, after preparation, we first shear the system over large strains (as large as 40 for the most adhesive systems with $u = 0.15$) before gathering any data, which we then record over similarly very large strains to detect any slow drift in the time series we record. We also perform measurements with different time origins to detect any such variation. Therefore all data presented below are representative stationary states.

III. MEASUREMENTS AND RESULTS

A. Repulsive particles

As discussed above, several recent experiments have suggested that jammed materials made of soft repulsive particles do not exhibit steady-state shear bands. For the system of harmonic spheres introduced by Durian to study wet foams [40], simulations have both reported the presence [48] or absence [50] of shear localization. The same model also displays strong dynamical heterogeneities under shear, similar to unsheared thermal glasses, quantified by measuring the usual dynamical susceptibility χ_4 [51]. Such heterogeneities have also been recently measured in the flow of NIPAM particles, which similarly interact solely via repulsive interactions [52]. Additionally, in the quasistatic limit the same model displays system-spanning avalanches [53] and strongly nonaffine particle motion [54]. Therefore there are marked spatiotemporal fluctuations and nonaffine particle motion for this system under shear flow, which certainly need to be taken into account when discussing velocity profiles and their fluctuations.

We begin to explore kinetic heterogeneities by looking at the map of nonaffine displacements of the particles, defined as deviations from the local single-particle displacements expected from assuming a linear velocity profile. The study of steady-state flow curve is delayed to Sec. IV. In the left panel of Fig. 2, we show such a map corresponding to a measurement done within a strain window of $\Delta\gamma = 0.10$ during steady-state flow at an imposed strain rate of $\dot\gamma = 2.5\times10^{-5}$, while the right panel shows the corresponding velocity profile. One can clearly observe the spatial heterogeneities in the dynamics with regions having different mobilities within this period of deformation. Moreover, this map suggests that the particles which have undergone large displacements cluster together to form a "band" aligned in the flow direction, similar to what has been, for instance, observed in amorphous Lennard-Jones solids under quasistatic deformation [23], at finite shear rates at $T = 0$ [55], or in supercooled liquids [56]. Quite often, the appearance of such system-spanning heterogeneities are invoked as proof of presence of "shear bands."

The spatial variation of mobilities, observed during this strain window $\Delta\gamma$, should also be reflected in the velocity profiles measured during the same interval. Indeed it does. The velocity profile measured during the same strain window when the above map was generated is shown in the right panel of Fig. 2. The region of large mobility in the map corresponds to a large deviation from a linear velocity profile.

A number of velocity profiles, all measured during independent strain windows of $\Delta\gamma = 0.10$ during steady-state flow at

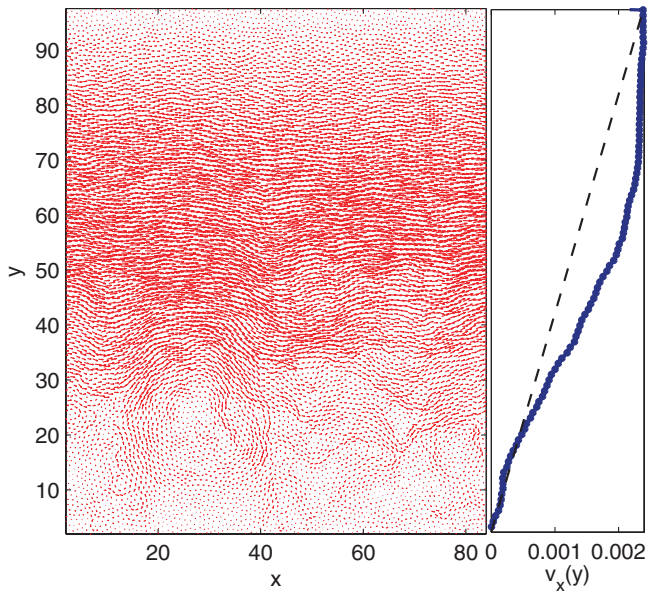

FIG. 2. (Color online) Left: Map of nonaffine displacements for repulsive particles, measured for an imposed shear rate of $\dot{\gamma} = 2.5 \times 10^{-5}$ and during a strain window of $\Delta\gamma = 0.10$ taken during steady-state flow. Right: The corresponding velocity profile, measured during the same strain window. The dashed line shows the velocity profile expected for a linear flow. A clear band can be observed near the middle of the system, which spans the system horizontally, but it is not permanent.

the same value of the shear rate are shown in Fig. 3. Large fluctuations deviating away from the expected linear velocity profile are generically observed. However, during flow the location of the more mobile region is seen to switch from one place to another, and the observed "shear bands" are in fact not permanent but have their own dynamics. Moreover, we do not always see a clear "coexistence" between two distinct regions of mobility, which is often associated with shear banding. Instead, the velocities might sometimes evolve more gradually across the channel.

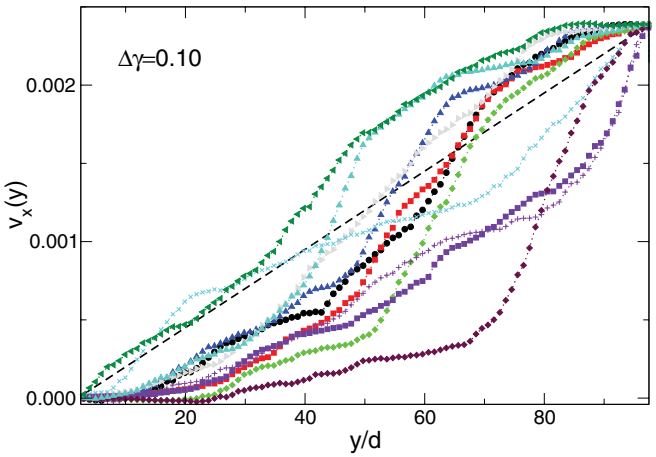

FIG. 3. (Color online) A series of representative velocity profiles for repulsive particles, averaged during a strain window of $\Delta\gamma = 0.10$, and sampled during steady-state flow at an imposed $\dot{\gamma} = 2.5 \times 10^{-5}$. These profiles reveal strong deviations from linear profiles, which strongly fluctuate both in space and time.

The observation of velocity profiles suggests that before drawing conclusions about the presence of shear localization it is necessary to study and quantify more precisely the degree of fluctuations of the velocity profiles, in order to answer the following two questions: How do the observed heterogeneities depend on the strain window chosen to average the profile? How do these fluctuations depend on the imposed macroscopic shear rate? We feel that such quantitative information is mandatory when reporting on shear-banding phenomena.

To analyze these fluctuations, we average the velocities in the x direction to compute the local strain rates $\dot{\gamma}(y)$ averaged over a given strain window $\Delta\gamma$. One can then construct, for any chosen $\Delta\gamma$, a histogram of these locally observed strain rates, which we denote $N(\dot{\gamma})$. Clearly this probability distribution function depends on the two key parameters whose influence we wish to study, namely the strain window $\Delta\gamma$ and the macroscopically imposed shear rate $\dot{\gamma}$.

We first show the evolution of $N(\dot{\gamma})$ with the strain window for a fixed value of the shear rate, $\dot{\gamma} = 5 \times 10^{-5}$, in the top panel of Fig. 4. For small strain intervals, $\Delta\gamma = 0.04$–0.10, $N(\dot{\gamma})$ spans across a wide range of local strain rates from nearly immobile regions ($\dot{\gamma} \sim 10^{-8}$) to regions which flow faster ($\dot{\gamma} \sim 3 \times 10^{-4}$) than the imposed shear rate. Moreover, the shape of the distribution is clearly not symmetric and

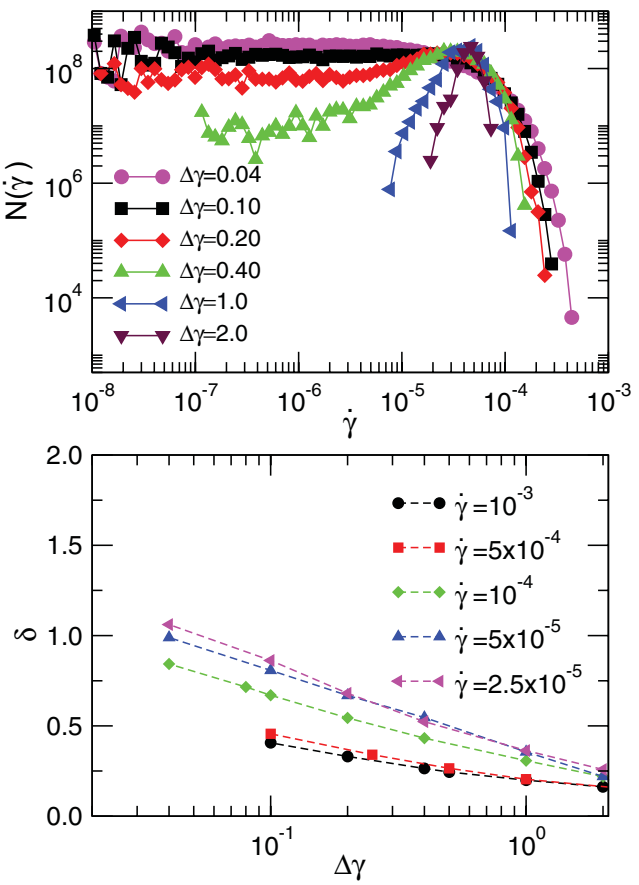

FIG. 4. (Color online) Top: Distribution of local strain rates $\dot{\gamma}(y)$ with changing the strain window $\Delta\gamma$ used for the average, at an imposed strain rate of 5×10^{-5}. Bottom: Variation of δ, Eq. (3), which quantifies the spread of the distribution $N(\dot{\gamma})$, with the strain window $\Delta\gamma$, for a range of imposed strain rates.

non-Gaussian, with the appearance of a flat tail toward small values of the shear rate. This behavior is clearly consistent with our observation that spatial fluctuations in the profiles, shown in Fig. 3, actually span the entire system. However, the distribution narrows down and becomes closer to a Gaussian with an increase of the strain window over which velocity profiles are averaged, suggesting that spatial fluctuations become less correlated over time. For the largest deformation, $\Delta\gamma = 2$, the fluctuations around the imposed shear rate have become quite small. Our observations are similar to what was reported for a sheared Lennard-Jones glass [57]. For small times, only a few plastic events occur resulting in the initial large heterogeneities which are localized in space. However, if one waits long enough, the plastic events proliferate across the system and the heterogeneities therefore are erased, which eventually results in homogeneous flow. Intriguingly, such description of the transient character of shear inhomogeneities is also reminiscent of the temporal evolution of kinetic heterogeneities characterizing the structural relaxation of thermal glassy systems [16].

These results suggest that some form of shear banding exists in the present system, but flow localization is not a permanent phenomenon. It is thus natural to ask about the lifetime of these inhomogeneities. To this end, we introduce the "dispersity" δ of the distribution $N(\dot{\gamma})$, as the ratio of the standard deviation to the mean of the distribution:

$$\delta = \frac{\sqrt{\langle \dot{\gamma}^2 \rangle_N - \langle \dot{\gamma} \rangle_N^2}}{\langle \dot{\gamma} \rangle_N}, \tag{3}$$

where the average $\langle \cdots \rangle_N$ is performed over the probability distribution of the local shear rate, $N(\dot{\gamma})$. The dispersity δ is the most natural way to quantify the width of this distribution.

In the bottom panel of Fig. 4, we show the variation of δ with the strain interval $\Delta\gamma$ for a range of imposed shear rates from $\dot{\gamma} = 2.5 \times 10^{-5}$ to 10^{-3}. Following from our discussion above, we find that δ decreases with $\Delta\gamma$ for all $\dot{\gamma}$. Therefore, if one averages the velocities for long enough strain windows, say larger than $\Delta\gamma \sim 2$, nearly linear velocity profiles will be observed in all cases. In fact, it is interesting to note that for all values of $\dot{\gamma}$, heterogeneities become negligible at approximately the same strain interval $\Delta\gamma$. However, in the regime of smaller $\Delta\gamma$, we see that flows become more heterogeneous with decreasing shear rates.

From these results, we conclude that our model of a jammed system with soft repulsive interactions does not produce permanent shear localization, although strong flow inhomogeneities are detected when insufficient averaging of the velocity profiles is performed, which might be a relevant issue in experiments. This analysis also suggests that a discussion of shear banding in soft jammed materials cannot be separated from a discussion of their spatiotemporal dynamics. In particular, we have presented in Fig. 4 a simple method to quantify the lifetime of these inhomogeneities. In Sec. IV we will relate these observations to the global rheology of the system.

B. Including attractive interactions

Motivated by recent experimental results [8,9] where the inclusion of particle adhesion in dense emulsions resulted in qualitatively different flow patterns compared to repulsive emulsions, we proceeded to explore the nature of flow heterogeneities in sheared soft disks with the tunable attractive interactions shown in Fig. 1.

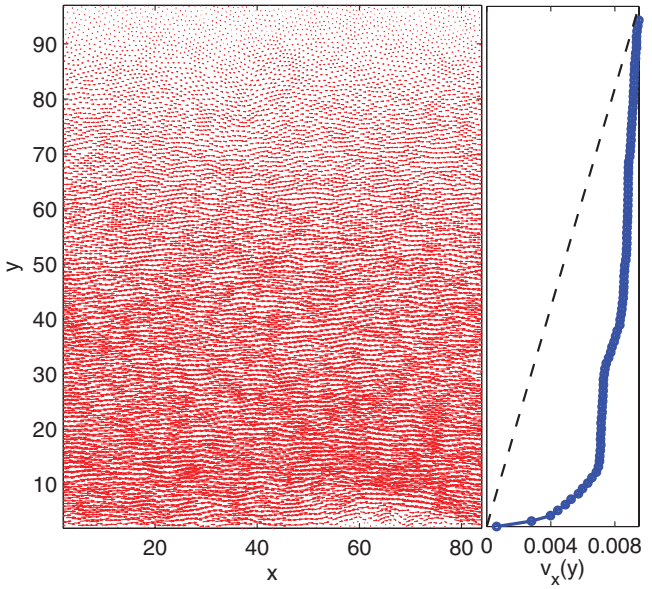

FIG. 5. (Color online) Left: Map of nonaffine displacements for attractive particles, $u = 0.15$, measured for an imposed shear rate of $\dot{\gamma} = 10^{-4}$ and during a strain window of $\Delta\gamma = 0.10$ taken during steady-state flow. Right: The corresponding velocity profile, measured during the same strain window. The dashed line shows the velocity profile expected for a linear flow. Compared with Fig. 2, the flow is much more inhomogeneous, the top 80% of the system being nearly unsheared, while the bottom part near the wall is sheared very strongly.

For these sticky particles, we again look at the map of nonaffine displacements. In the left panel of Fig. 5, we show the spatial map of such displacements for $u = 0.15$ during a strain interval of $\Delta\gamma = 0.10$, measured in steady state at an imposed shear rate of $\dot{\gamma} = 10^{-4}$. The corresponding velocity profile is shown in the right panel of Fig. 5. In the bottom of the map, we can again very clearly see a band formed by the most mobile particles, which spans across the entire length of the system in the flow direction, and having a transverse width of around 10–20 diameters, while the top of the system is mainly unsheared. The corresponding velocity profile also reflects this via its strongly nonlinear shape in the entire system. More interestingly, the mobile band populates the bottom of the shear cell adjacent to the static wall, whereas the quiet ones are adjacent to the top wall of the cell via which shear is generated across the cell, which is also evident from the corresponding velocity profile.

This is further illustrated by looking at a set of consecutive velocity profiles measured during the same strain window, $\Delta\gamma = 0.10$, as shown in the top panel of Fig. 6. We observe quite dramatic deviations from a linear velocity profile in all cases and one can clearly see a switching of the position of the more mobile population with time as the shear band continuously flips from one wall to the other. Note that the shear rate at the center of the channel is always very small, such that the bulk of the system either flows with the right wall,

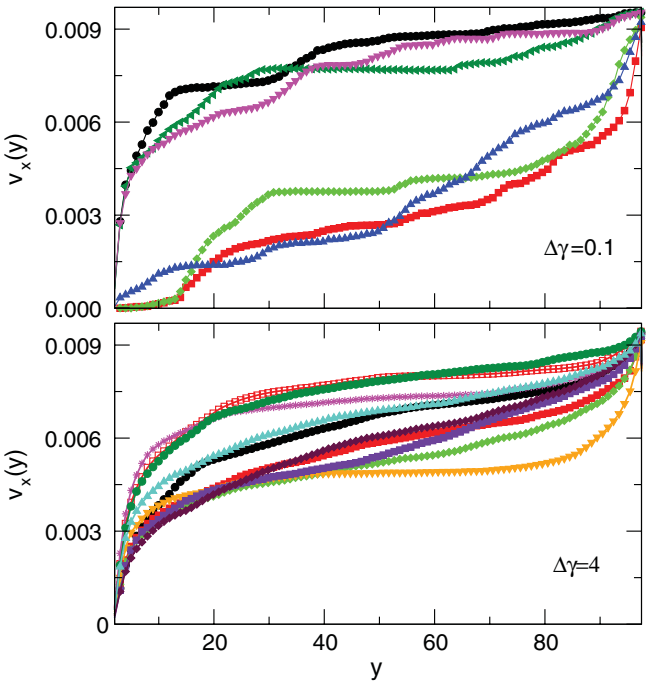

FIG. 6. (Color online) A series of representative velocity profiles for attractive particles with $u = 0.15$, averaged during a strain window of $\Delta\gamma = 0.10$ (top), and $\Delta\gamma = 4.0$ (bottom), and sampled during steady-state flow at an imposed shear rate $\dot{\gamma} = 10^{-4}$. These profiles reveal strong deviations from linear profiles, which strongly fluctuate both in space and time. Compared to the repulsive system, these profiles remain strongly nonlinear at large deformation $\Delta\gamma = 4.0$, suggesting that a linear velocity profile is not stable in the presence of strong particle adhesion.

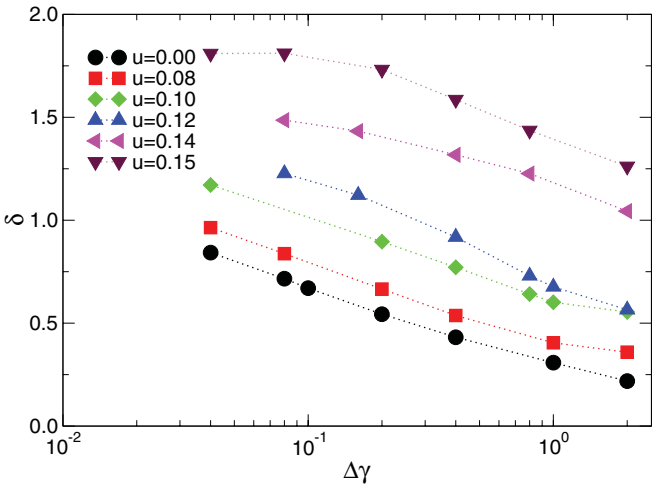

FIG. 7. (Color online) Effect of particle attraction on the variation of the dispersity δ, Eq. (3), which quantifies the spread of the distribution $N(\dot{\gamma})$, with the strain window $\Delta\gamma$, for an imposed shear rate of $\dot{\gamma} = 10^{-4}$. Attraction enhances both the amplitude and the lifetime of the flow heterogeneities.

or remains immobile with the left wall. Although seemingly reminiscent of the velocity oscillations reported for colloidal particles in microchannels [58], the motion we observe with attractive particles is instead very far from periodic, and it is enhanced by low rather than fast shear rates.

When averaged over a much longer period, $\Delta\gamma = 4$, the velocity profiles still deviate significantly from linear profiles, as shown in the bottom panel of Fig. 6. For the profiles measured during this period, the central region appears nearly unsheared, whereas the regions close to both the top and bottom walls show local shear rates which are larger than the imposed value. Thus the flow heterogeneities are much more pronounced in the attractive system, with much clearer signs of the "coexistence" between sheared and unsheared regions, and this inhomogeneity seems to be persistent over much longer strain intervals for the attractive systems as compared to the repulsive one.

Are these shear bands permanent objects? To answer this question for these sticky particles, we again characterize their lifetime, repeating the exercise performed for the repulsive particles. For each strength of attraction u, we compute local strain rates $\dot{\gamma}$ from velocity profiles averaged over different strain intervals $\Delta\gamma$. We build the corresponding histograms $N(\dot{\gamma})$ and measure the dispersity δ of the local strain rates from Eq. (3). Since the lifetime of the inhomogeneities becomes large when attraction increases, it becomes numerically difficult to sample a large number of independent fluctuations and get accurate statistics for the distributions. This forces us to impose a larger shear rate, $\dot{\gamma} = 10^{-4}$, because much longer simulations would be needed to obtain good statistics at lower shear rates, where, presumably, even longer lived and more pronounced heterogeneities are present.

The data for $\dot{\gamma} = 10^{-4}$ are shown in Fig. 7. We can distinctly see that for all strain intervals, increasing attraction between the particles results in increased heterogeneities. We suspect the effect would be even more pronounced for lower shear rates. In fact, within the strain windows that we have been able to sample, the heterogeneities have not died out when u is large enough. For instance, the dispersity obtained over an averaging window $\Delta\gamma = 2.0$ for $u > 0.12$ is larger than the dispersity for $u = 0$ and $\Delta\gamma = 0.1$. However, δ is still clearly a decreasing function of $\Delta\gamma$, which suggests that for even larger strain windows, the temporal fluctuations reported in Fig. 6 eventually decrease the overall width of the shear rate distribution $N(\dot{\gamma})$. While we conclude that there are no permanent shear bands in our jammed adhesive systems, our data are nevertheless in broad agreement with experimental results showing that particle adhesion strongly enhances localization of the shear [8–11], in the sense that our most adhesive systems do not sustain stable linear flow profiles, even when averaging velocities over deformations as large as 400%.

In the following section, we shall discuss the physical origin of these observations.

IV. DISCUSSION AND INTERPRETATION

A. Static and dynamic yield stresses

To understand the above observations and the effect of the attractive forces, we now turn to the global flow curve of the system and ask which (if any) of the theoretical arguments summarized in the introduction might apply to our system.

In Fig. 8, we show the flow curves $\sigma = \sigma(\dot{\gamma})$ obtained by averaging the stress over the entire system and very long

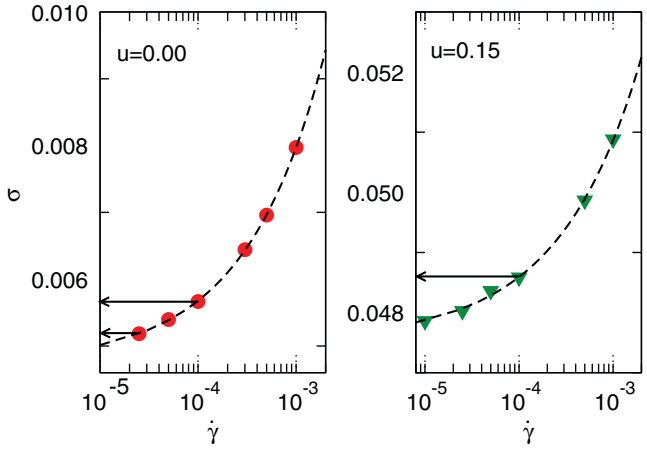

FIG. 8. (Color online) Global flow curves $\sigma = \sigma(\dot{\gamma})$ for the repulsive particles with $u = 0.0$ (left) and attractive particles with $u = 0.15$ (right). The data are shown with symbols, while the dashed lines are fits to the Herschel-Bulkley form, Eq. (4). Horizontal arrows indicate the stress values at which constant stress simulations are performed; see Figs. 9 and 10. Notice the very different stress scales used in both panels.

times in our simulations with various values of the imposed shear rates. We find similar results by studying temporally and spatially resolved quantities, suggesting our systems are not structurally heterogeneous. For both repulsive ($u = 0$) and strongly attractive ($u = 0.15$) interactions, we find that the resulting flow curves are monotonic functions, thus ruling out the possibility that nonmonotonic flow curves could arise in dense athermal systems with or without adhesive forces. Additionally, we find that all flow curves are well described by a Herschel-Bulkley fitting function, which we write as

$$\sigma_{\rm hb} = \sigma_d[1 + (\tau_c\dot{\gamma})^n], \tag{4}$$

which contains three fitting parameters. The first parameter is the dynamic yield stress σ_d, defined as the $\dot{\gamma} \to 0$ limit of the measured stress. The second parameter, n, determines the shear-thinning behavior observed for shear rates that are large enough to be away from the "yield regime" (defined by $\sigma \approx \sigma_d$). The third parameter, τ_c, has the dimensions of a time scale. It indicates at which imposed shear rate the flow is close to the yield regime, $\tau_c\dot{\gamma} \ll 1$, or far from it, $\tau_c\dot{\gamma} \gg 1$. The obtained values of these fitting parameters are further discussed in Sec. IV B.

In the study of the formation of shear bands in Lennard-Jones glass [17], evidence was found of a multivalued flow curve by including also the behavior of the system at rest, $\dot{\gamma} = 0$. This multivalued nature was due to the fact that the value of the static yield stress σ_s, determined by checking for the onset of flow by applying an increasing external stress on a quiescent amorphous state [47], was found to be higher than the dynamical yield stress σ_d defined from finite shear rates measurements. A strict inequality, $\sigma_s > \sigma_d$, indeed opens a stress window, $\sigma \in [\sigma_d,\sigma_s]$, where the system can either be at rest, $\dot{\gamma} = 0$, or flow at finite rate $\dot{\gamma} > 0$, with the possibility that both solutions coexist in space, thus possibly giving rise to flow inhomogeneities [18].

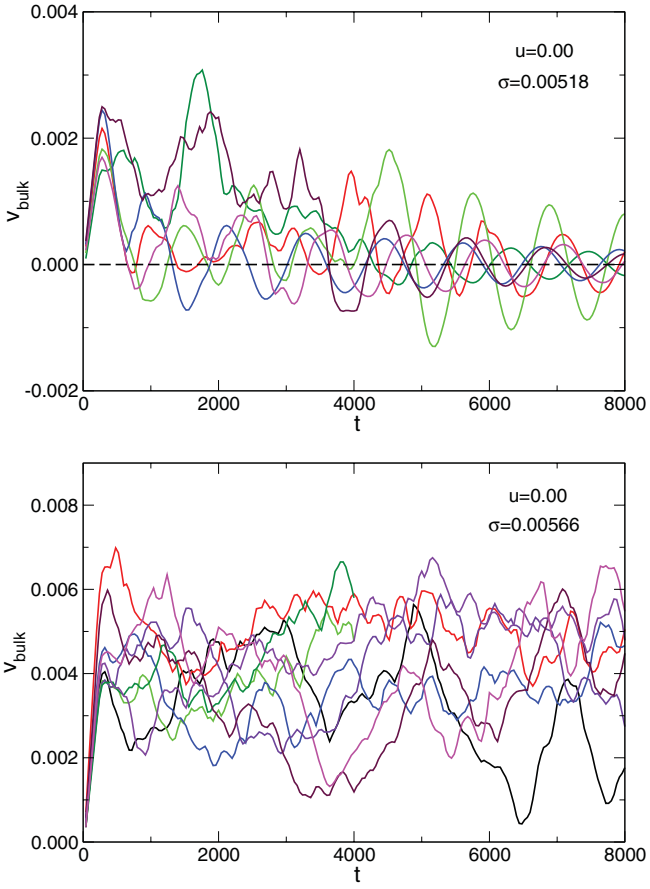

FIG. 9. (Color online) For repulsive particles, $u = 0$, velocity $v_{\rm bulk}$ of the center of mass of the system in the direction of the imposed shear stress starting from a configuration at rest. Different colors correspond to independent initial conditions. Comparison between both panels shows that the static yield stress lies in between the two simulated stress values, $\sigma = 0.005\,18 < \sigma_s < \sigma = 0.005\,66$.

Having ruled out nonmonotonic flow curves at finite shear rates, we thus decided to check whether this scenario is a possible explanation of the observed flow heterogeneities. Unfortunately, determining σ_s numerically is not an easy task [47]. To proceed, we performed simulations with an imposed constant stress σ to determine whether the static and dynamic yield stresses differ for our systems. By definition, the system should not flow when $\sigma < \sigma_s$.

Using the global flow curves shown in Fig. 8, we select for $u = 0$ two different values of stress to carry out our constant stress simulations. The first value is $\sigma = 0.005\,18$, which corresponds to $\dot{\gamma} = 2.5 \times 10^{-5}$. Second, we use $\sigma = 0.005\,66$, which corresponds to $\dot{\gamma} = 10^{-4}$. Both values are indicated with horizontal arrows in Fig. 8, and the results for these runs are presented in Fig. 9. To determine whether the system flows or not, we simply measure the average velocity $v_{\rm bulk}$ of the system in the direction of the applied stress. As initial conditions for these runs, we choose arrested states corresponding to local minima in the energy landscape of the soft disks.

The top panel in Fig. 9 shows that for all the different trajectories at $\sigma = 0.005\,18$, the motion of the fluid particles quantified by the average velocity $v_{\rm bulk}$ eventually stops at long times. On the contrary, for $\sigma = 0.005\,66$, the flow continues

at some finite velocity $v_{\rm bulk}$. Thus this tells us that σ_s lies in between these two stress values, and that indeed it is larger than the dynamic yield stress σ_d for this system. The situation is therefore similar to the observations reported for a Lennard-Jones glass [17]. The fact that there is no flow at $\sigma = 0.005\,18$ indicates why the heterogeneities are more significant during the simulations at $\dot\gamma = 2.5 \times 10^{-5}$, in comparison to the flow at $\dot\gamma = 10^{-4}$; see Fig. 4.

However, one should note that earlier numerical studies have reported that the difference between σ_s and σ_d seems to decrease (albeit quite slowly) as the system size is increased towards the thermodynamic limit [48,59]. Thus this indicates that the corresponding degree of flow heterogeneities could also have finite size effects, despite the fact that our systems already comprise a large number of particles, $N \approx 10^4$, and that the channel we use is about 100 particles wide. We also note the following paradox. Given that the length scale of kinetic heterogeneities grows as the shear rate decreases and is believed to diverge as $\dot\gamma \to 0$ in systems characterized by a yield stress [51], for any finite size system there should exist a shear rate below which finite size effects become relevant, and the mechanism mentioned above for the appearance of strong flow inhomogeneities could then become relevant as well.

We now switch to the attractive system with $u = 0.15$ and ask whether forcing the system with a stress value corresponding to $\dot\gamma = 10^{-4}$ induces flow in the system as it does for repulsive particles. The corresponding magnitude of the external stress, $\sigma = 0.048\,58$, is indicated by an arrow in the right panel of Fig. 8. The resulting data are plotted in Fig. 10, and should be compared to the bottom panel of Fig. 9. We observe that for all initial states, the system eventually comes to rest. Thus, in this case, the static yield stress σ_s is larger than the shear stress corresponding to $\dot\gamma = 10^{-4}$. This result is in agreement with our earlier observation that at this shear rate, attractive systems display much stronger flow inhomogeneities than repulsive ones; recall Fig. 7.

Therefore we conclude from this section that the existence of distinct values for static and dynamic yield stresses accounts well for flow inhomogeneities in our system, as opposed to a nonmonotonic flow curve at finite shear rates. Moreover, we also showed that the stress window where this competition becomes relevant corresponds to shear rates values that become larger when attraction is increased, as shown by our constant stress simulations. We finally remark that these latter results suggest that by making simulations at constant shear stress, the fluid velocity would remain zero as long as $\sigma < \sigma_s$, and would jump discontinuously to a finite value at σ_s. This is nothing but the "viscosity bifurcation" observed in several experiments [9,60,61]. In this language, our results imply that increasing the attraction increases the value of the "critical" shear rate $\dot\gamma_c$ at which a steady-state flow appears, which seems consistent with experimental results [11].

Thus we come to the conclusion that the effect of particle adhesion is to continuously increase the critical shear rate above which stable linear profiles exist. Therefore, for adhesive particles, the regime below the critical shear rate becomes easily accessible in numerical simulations, leading to observation of more prominent inhomogeneities in flow. However, we do not obtain numerical evidence that some novel physics comes in, such as, for instance, a slower restructuration process, as advocated in Refs. [36–38]. We now seek a more microscopic explanation of these effects.

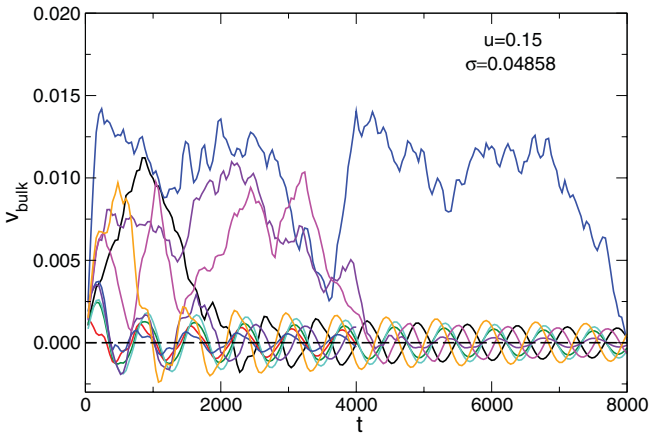

FIG. 10. (Color online) Same as Fig. 9 for attractive particles, $u = 0.15$, and a stress value shown with a horizontal arrow in Fig. 8 corresponding to $\dot\gamma = 10^{-4}$. For all initial states, the system remains at rest, showing that $\sigma_s > 0.048\,58$.

B. "Universal" rescaling of flow curves

We thus see the emergence of a universal scenario for the existence of flow heterogeneities, irrespective of the interparticle interactions. First, we observed that for both attractive or repulsive interactions, the heterogeneous flow corresponds to the regime bounded by values of static and dynamic yield stresses. Moreover, the flow curves for all the different systems ($u = 0.0, 0.05, 0.10, 0.15$) are well fitted with the same functional form, Eq. (4). We find empirically that the shear-thinning exponent n varies very little around the value $n \approx 0.5$ with no systematic trend. Thus we fix $n = \frac{1}{2}$ in the following and determine σ_d and τ_c from a fit to the data. This analysis thus suggests that the flow curves for all our systems can be collapsed by using the scaled variables

$$y = \frac{\sigma}{\sigma_d}; \quad x = \tau_c \dot\gamma; \tag{5}$$

onto the simple functional form:

$$y = 1 + \sqrt{x}. \tag{6}$$

This procedure is applied in Fig. 11, where the two insets display the evolution with the strength of the attraction of the two parameters σ_d and τ_c obtained by fitting the flow curves.

We find that the yield stress σ_d increases with the attraction u, which is expected as the attraction should indeed make the emulsion more cohesive and harder to deform. A more surprising result is that the time scale τ_c is found to decrease dramatically by about two orders of magnitude between $u = 0$ and $u = 0.15$. We shall dwell on this unexpected result in the following section.

The significant observation following the data collapse shown in Fig. 11 is that, for the range of imposed shear rates explored in our simulations, the data points corresponding to increasing attraction correspond to dramatically decreasing values of the scaled variable $x = \tau_c \dot\gamma$ in the master curve.

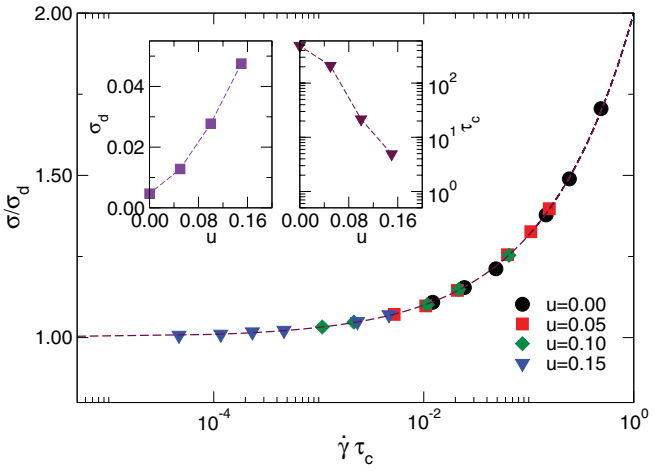

FIG. 11. (Color online) Scaled representation of the flow curves for all parameters, using the scaled variables in Eq. (5). The dashed line is the simple functional form in Eq. (6). Inset: Variation of the dynamic yield stress σ_d (left), and of the time scale τ_c (right) with the strength of the attractive forces u.

Thus varying the degree of attraction allows us to "slide" along this master curve, so that the most attractive system is effectively much closer to the yield stress regime, where strongly heterogeneous flow can be expected. On the other hand, repulsive particles correspond to a more fluidized segment of the flow curve, which explains why only relatively short-lived inhomogeneities are observed in that case.

While framing their model for shear banding in Ref. [36], the authors obtained a similar rescaling of experimental data for varying degrees of loaded emulsions. However, they attribute an increasing tendency toward shear banding to an increasing time scale for "restructuration" of the material under shear with higher degree of loading (stickiness), which is a trend opposite to what we observe here. For clarity, we should emphasize again that at the large value of the volume fraction ($\phi = 1.0$) that we have studied here, the material is not a gel but a highly homogeneous material. For this reason, we believe that local fluctuations in the volume fraction are not significant, which also rules out the flow-concentration coupling scenario proposed in another model [39] for our jammed systems. We also notice that similar collapse of flow curves often occurs in soft glassy materials [62], although in our case thermal fluctuations cannot be used to account for the behavior of τ_c.

The above analysis implies that varying the attraction changes the nature of inhomogeneities by affecting the scaled variable $x = \tau_c\dot{\gamma}$ through the evolution of τ_c. Clearly, the same result would be obtained by varying instead the shear rate for a given value of τ_c. This reasoning is consistent with the data shown in Fig. 4, which established that inhomogeneities increase when the shear rate decreases.

C. Microscopic interpretation of time scale τ_c

The final piece of information that we need to gather is a microscopic understanding of the strong variation with the strength of attractive forces of the intrinsic time scale τ_c appearing in the global flow curves, Eq. (4). Under an applied shear, the system constantly renews its structure. We believe that τ_c quantifies the time scale needed for the local stress relaxation to occur. Thus when the typical time scale $1/\dot{\gamma}$ associated with the imposed shear flow is much slower than τ_c, i.e., when $\tau_c\dot{\gamma} \ll 1$, the system is effectively in the near quasistatic regime, and $\sigma \approx \sigma_d$. In the opposite regime, $\tau_c\dot{\gamma} \gg 1$, the system has not enough time to relax the stress whose averaged value increases above the yield stress.

In this view, τ_c is a time scale associated to relaxation of the stress after deformation. To confirm this interpretation, we conduct the following numerical experiment. For the different values of attraction from $u = 0$ to $u = 0.15$, we apply an instantaneous external strain in the x direction of magnitude Γ, starting from an initially relaxed state (which corresponds to a local minima in the energy landscape). We then allow this strained configuration to relax [63,64]. To fix the value of Γ, we seek a compromise between a very small value where only trivial elastic deformation would occur, and a very large value which would amount to starting from a fully random configuration. We have studied two values, $\Gamma = 0.1$ and $\Gamma = 0.2$, because they typically correspond to the magnitude of the strain where plastic deformations occur in quasistatic simulations [53]. We find similar results in both cases and show results obtained for $\Gamma = 0.2$.

We present our data for stress relaxation after these step strains in Fig. 12, where each curve is averaged over several (typically ten) initial states. To ease the comparison between different values of the attraction, we plot $\sigma(t)/\sigma(0)$, where $\sigma(0)$ is the stress value right after the step strain has been imposed.

Several remarks can be made based on this figure. Altogether the stress exhibits a first rapid decay, followed by a plateau at long time scale. First, the short time scale for the stress relaxation is observed to decrease strongly with increasing the attraction strength. This is in line with the result for the time scale τ_c in Fig. 11. However, if we estimate a typical decay time from the data shown in Fig. 12, we find that its variation with attraction is slightly less (a factor of 100 instead of 200) than the one of τ_c, suggesting that these

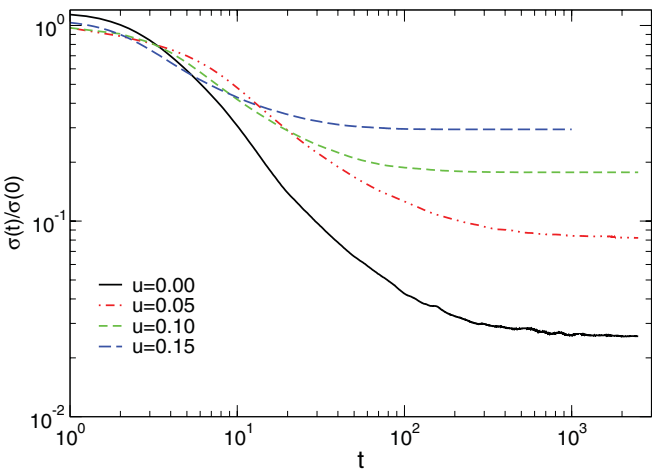

FIG. 12. (Color online) Relaxation of the stress after a step strain of amplitude $\Gamma = 0.2$ for the different strengths of interaction u. The amount of relaxed stress and the time scale for relaxation both decrease strongly with increasing the attraction u.

two times might share a common origin but capture distinct relaxation processes.

Second, it is evident that the degree of stickiness influences the amount of stress that is relaxed after the step strain, which becomes smaller for stronger adhesion: stickiness increases the amount of residual stress that the system can store. A possible interpretation is that after deformation adhesive particles very rapidly "stick" to the neighboring particles to minimize locally the potential energy, and remain subsequently in this local minimum, while more collective, slower moves relaxing larger amounts of stress are more likely to occur for purely repulsive particles.

In the present system, shear localization is enhanced by adhesion because attractive forces accelerate the time scale for restructuration after deformation, thus effectively moving the system closer to the quasistatic, yield stress regime where heterogeneities are more pronounced. Furthermore the increase of residual stresses for adhesive particles does stabilize the transient shear bands over longer times.

V. CONCLUSION

We carried out simulations of two-dimensional jammed systems to study the nature of shear flow heterogeneities and the influence of the degree of attractive interaction between particles. We demonstrated that, independently of the nature of interactions, the flow behavior could be described by a universal flow curve, with increasing attraction resulting in a flow which is more and more influenced by the proximity to the yield stress regime. By entering a regime of stress values bounded by the static and dynamic yield stress, shear localization is strongly promoted, and with increasing attraction, one observes enhanced and very long-lived flow inhomogeneities. For the most strongly adhesive particles, we find that velocity profiles do not become linear even when averaged over very large deformations, suggesting that in these systems a linear flow profile is actually unstable. However, these inhomogeneities do not take the form of simple, permanent shear bands. We believe that these general conclusions are not specific to two dimensions but would carry over to three dimensions.

Our results are reminiscent of long-lived flow inhomogeneities measured experimentally in simple yield stress fluids [7]. Interestingly, similar to our adhesive soft system, carbopol is measured to exhibit a monotonic Herschel-Bulkley flow curve [7], and does not exhibit thixotropy or aging. An important difference is that the experiments report long transients when the shear is turned on, while we worked here in steady state. On the theoretical side, similar conclusions about the transient nature of shear bands were reached in Refs. [21,32,33] on the basis of spatially resolved coarse-grained models using the idea that after long aging the static yield stress value can become appreciably larger than the dynamic yield stress. We emphasize that, in contrast to these works, the distinct values for these two yield stresses we report here do not depend on the aging time since our systems are fully athermal.

By contrast, fully permanent flow localization taking the form of simple shear bands has been predicted through several mesoscopic models [29,34,36–38], which all attempt to describe a self-consistent coupling of the yielding mechanism to the structural reorganization (e.g., softening mechanisms, time-scales separation in the structural relaxation, etc.). While these descriptions lead to the occurrence of permanent bands, this flow behavior is systematically associated with the appearance of a nonmonotonic behavior of the flow curve $\sigma(\dot{\gamma})$ at finite shear rate. Although experimental results, simulations, and the various theoretical models all suggest that this nonmonotonicity is a necessary condition to observe permanent shear bands, we demonstrate here that very long-lived, strongly nonlinear flow profiles can be observed without it.

Clearly, to make progress and to go beyond the above observations and conflicting predictions, it would be desirable to make explicit connections between the microscopic physical parameters in experiments or simulations—such as the adhesive forces considered in this work—and the mesoscopic phenomenological quantities introduced in the various simplified theoretical models, such as, for instance, the distinct time scales which enter the definition of coarse-grained elastoplastic models [36–38], or the effective "noise" temperature in the SGR models and its numerous variants [32,34].

Altogether, our results suggest that "shear localization" actually denotes a broad variety of physical behaviors, and further experiments performed with controlled model systems with tunable adhesion would be required to investigate the intimate connection between structural recovery and shear localization along the lines of the present work. Similarly, it would be interesting to design a simple microscopic model yielding the type of permanent shear bands envisioned by coarse-grained models, for instance, by studying simple atomistic models for colloidal gels.

ACKNOWLEDGMENTS

We thank ANR SYSCOM for financial support and C. Barentin, J.-L. Barrat, A. Colin, T. Divoux, C. Heussinger, and K. Martens for useful discussions.

[1] M. van Hecke, J. Phys.: Condens. Matter **22**, 033101 (2010).
[2] P. Coussot, *Rheometry of Pastes, Suspensions, and Granular Materials* (Wiley, New York, 2005).
[3] P. Coussot, Soft Matter **3**, 528 (2007).
[4] P. Schall and M. van Hecke, Annu. Rev. Fluid Mech. **42**, 67 (2010).
[5] G. Ovarlez, S. Rodts, X. Chateau, and P. Coussot, Rheol. Acta **48**, 831 (2009).
[6] G. Ovarlez, K. Krishan, and S. Cohen-Addad, Europhys. Lett. **91**, 68005 (2010).
[7] T. Divoux, D. Tamarii, C. Barentin, and S. Manneville, Phys. Rev. Lett. **104**, 208301 (2010).

[8] L. Bécu, S. Manneville, and A. Colin, Phys. Rev. Lett. **96**, 138302 (2006).
[9] A. Ragouilliaux, G. Ovarlez, N. Shahidzadeh-Bonn, B. Herzhaft, T. Palermo, and P. Coussot, Phys. Rev. E **76**, 051408 (2007).
[10] G. Ovarlez, S. Rodts, A. Ragouilliaux, P. Coussot, J. Goyon, and A. Colin, Phys. Rev. E **78**, 036307 (2008).
[11] A. Fall, J. Paredes, and D. Bonn, Phys. Rev. Lett. **105**, 225502 (2010).
[12] P. Moller, A. Fall, V. Chikkadi, D. Derks, and D. Bonn, Philos. Trans. R. Soc. A **367**, 5139 (2009).
[13] P. C. F. Moller, S. Rodts, M. A. J. Michels, and D. Bonn, Phys. Rev. E **77**, 041507 (2008).
[14] D. Bonn and M. D. Denn, Science **324**, 1401 (2009).
[15] J.-L. Barrat and A. Lemaitre, Dynamical Heterogeneities in Glasses, Colloids, and Granular Materials (Ref. [16]), Chap. 8; e-print arXiv:1009.5774.
[16] *Dynamical Heterogeneities in Glasses, Colloids and Granular Materials*, edited by L. Berthier, G. Biroli, J.-P. Bouchaud, L. Cipelletti, and W. van Saarloos (Oxford University Press, Oxford, 2011).
[17] F. Varnik, L. Bocquet, J.-L. Barrat, and L. Berthier, Phys. Rev. Lett. **90**, 095702 (2003).
[18] L. Berthier, J. Phys.: Condens. Matter **15**, S933 (2003).
[19] Y. Shi and M. L. Falk, Phys. Rev. Lett. **95**, 095502 (2005); Phys. Rev. B **73**, 214201 (2006).
[20] M. L. Falk and J. S. Langer, Phys. Rev. E **57**, 7192 (1998).
[21] M. L. Manning, J. S. Langer, and J. M. Carlson, Phys. Rev. E **76**, 056106 (2007).
[22] C. Maloney and A. Lemaitre, Phys. Rev. Lett. **93**, 195501 (2004); Phys. Rev. E **74**, 016118 (2006).
[23] A. Tanguy, F. Leonforte, and J.-L. Barrat, Eur. Phys. J. E **20**, 355 (2006).
[24] P. Sollich, F. Lequeux, P. Hebraud, and M. E. Cates, Phys. Rev. Lett. **78**, 2020 (1997)
[25] P. Hébraud and F. Lequeux, Phys. Rev. Lett. **81**, 2934 (1998).
[26] L. Berthier, J.-L. Barrat, and J. Kurchan, Phys. Rev. E **61**, 5464 (2000).
[27] G. Picard, A. Ajdari, F. Lequeux, and L. Bocquet, Phys. Rev. E **71**, 010501 (2005).
[28] J. C. Baret, D. Vandembroucq, and S. Roux, Phys. Rev. Lett. **89**, 195506 (2002).
[29] E. A. Jagla, Phys. Rev. E **76**, 046119 (2007).
[30] K. Martens, L. Bocquet, and J.-L. Barrat, Phys. Rev. Lett. **106**, 156001 (2011).
[31] L. Bocquet, A. Colin, and A. Ajdari, Phys. Rev. Lett. **103**, 036001 (2009).
[32] R. L. Moorcroft, M. E. Cates, and S. M. Fielding, Phys. Rev. Lett. **106**, 055502 (2011).
[33] D. Vandembroucq and S. Roux, Phys. Rev. B **84**, 134210 (2011).
[34] S. M. Fielding, M. E. Cates, and P. Sollich, Soft Matter **5**, 2378 (2009).
[35] P. Sollich, Phys. Rev. E **58**, 738 (1998).
[36] P. Coussot and G. Ovarlez, Eur. Phys. J. E **33**, 183 (2010).
[37] V. Mansard, A. Colin, P. Chaudhuri, and L. Bocquet, Soft Matter **7**, 5524 (2011).
[38] K. Martens, L. Bocquet, and J.-L. Barrat (in press), e-print arXiv:1111.0581.
[39] R. Besseling, L. Isa, P. Ballesta, G. Petekidis, M. E. Cates, and W. C. K. Poon, Phys. Rev. Lett. **105**, 268301 (2010).
[40] D. J. Durian, Phys. Rev. Lett. **75**, 4780 (1995); Phys. Rev. E **55**, 1739 (1997).
[41] M. Lundberg, K. Krishan, N. Xu, C. S. O'Hern, and M. Dennin, Phys. Rev. E **79**, 041405 (2009).
[42] C. S. O'Hern, S. A. Langer, A. J. Liu, and S. R. Nagel, Phys. Rev. Lett. **88**, 075507 (2002);
[43] C. S. O'Hern, L. E. Silbert, A. J. Liu, and S. R. Nagel, Phys. Rev. E **68**, 011306 (2003).
[44] L. Berthier and T. A. Witten, Europhys. Lett. **86**, 10001 (2009); Phys. Rev. E **80**, 021502 (2009).
[45] G. Lois, J. Blawzdziewicz, and C. S. O'Hern, Phys. Rev. Lett. **100**, 028001 (2008).
[46] J. Goyon, A. Colin, G. Ovarlez, A. Ajdari, and L. Bocquet, Nature (London) **454**, 84 (2008).
[47] F. Varnik, L. Bocquet, and J.-L. Barrat, J. Chem. Phys. **120**, 2788 (2004).
[48] N. Xu and C. S. O'Hern, Phys. Rev. E **73**, 061303 (2006).
[49] R. Groot and P. Warren, J. Chem. Phys. **107**, 4423 (1997).
[50] V. J. Langlois, S. Hutzler, and D. Weaire, Phys. Rev. E **78**, 021401 (2008).
[51] C. Heussinger, P. Chaudhuri, and J.-L. Barrat, Soft Matter **6**, 3050 (2010).
[52] K. N. Nordstrom, J. P. Gollub, and D. J. Durian, Phys. Rev. E **84**, 021403 (2011).
[53] C. Heussinger and J.-L. Barrat, Phys. Rev. Lett. **102**, 218303 (2009).
[54] C. Heussinger, L. Berthier, and J.-L. Barrat, Europhys. Lett. **90**, 20005 (2010).
[55] A. Lemaitre and C. Caroli, Phys. Rev. Lett. **103**, 065501 (2009).
[56] A. Furukawa, K. Kim, S. Saito, and H. Tanaka, Phys. Rev. Lett. **102**, 016001 (2009).
[57] H. Shiba and A. Onuki, Phys. Rev. E **81**, 051501 (2010).
[58] L. Isa, R. Besseling, A. N. Morozov, and W. C. K. Poon, Phys. Rev. Lett. **102**, 058302 (2009).
[59] P.-E. Peyneau and J.-N. Roux, Phys. Rev. E **78**, 011307 (2008).
[60] P. Coussot, J. S. Raynaud, F. Bertrand, P. Moucheront, J. P. Guilbaud, H. T. Huynh, S. Jarny, and D. Lesueur, Phys. Rev. Lett. **88**, 218301 (2002).
[61] F. Da Cruz, F. Chevoir, D. Bonn, and P. Coussot, Phys. Rev. E **66**, 051305 (2002).
[62] M. Cloitre, R. Borrega, F. Monti, and L. Leibler, Phys. Rev. Lett. **90**, 068303 (2003).
[63] T. Hatano, Phys. Rev. E **79**, 050301 (2009).
[64] J. Zausch and J. Horbach, Europhys. Lett. **88**, 60001 (2009).